Final Report

Title: Towards the concept of Design for In-situ Structural Health Monitoring (DISHMo)

AFOSR/AOARD Reference Number: AOARD-09-4036

AFOSR/AOARD Program Manager: Dr Kumar Jata.

Period of Performance: 28 September 2009 – 27 September 2010

Submission Date: September 2010

PI: W.K. Chiu, Monash University
F.K. Chang, Stanford University
N. Rajic, DSTO, Australia

Report Documentation Page

Form Approved
OMB No. 0704-0188

1. REPORT DATE	2. REPORT TYPE	3. DATES COVERED
05 FEB 2011	**FInal**	**26-03-2009 to 26-09-2010**

4. TITLE AND SUBTITLE
Towards the concept of Design for In-Situ Structural Health Monitoring (DISHMo)

5a. CONTRACT NUMBER
FA23860914036

5b. GRANT NUMBER

5c. PROGRAM ELEMENT NUMBER

6. AUTHOR(S)
Wing Kong Chiu

5d. PROJECT NUMBER

5e. TASK NUMBER

5f. WORK UNIT NUMBER

7. PERFORMING ORGANIZATION NAME(S) AND ADDRESS(ES)
Monash University,P.O. Box 31, Monash University, Wellington Road,Clayton, Victoria 3800,Australia,AU,3800

8. PERFORMING ORGANIZATION REPORT NUMBER
N/A

9. SPONSORING/MONITORING AGENCY NAME(S) AND ADDRESS(ES)
AOARD, UNIT 45002, APO, AP, 96337-5002

10. SPONSOR/MONITOR'S ACRONYM(S)
AOARD

11. SPONSOR/MONITOR'S REPORT NUMBER(S)
AOARD-094036

12. DISTRIBUTION/AVAILABILITY STATEMENT
Approved for public release; distribution unlimited

13. SUPPLEMENTARY NOTES

14. ABSTRACT

A significant amount of research work has been dedicated towards structural health monitoring (SHM). Much of this work is targeted towards the introduction of the monitoring techniques to existing structures. To fully exploit the benefits of structural health monitoring, the application of these monitoring techniques must be addressed at the design stage. The work reported on in this report outlines a series of works that were devoted to the understanding how structural geometry can be designed to facilitate the Lamb wave based SHM. This report also describes a computationally efficient optical approach to studying the propagation of Lamb waves in a plate-like structure. This analytical tool was used to visualize the flow of the Lamb wave energy to aid in the design of geometrically varying structural features for efficient structural health monitoring. Compared with flat plates, plate-like structures with geometry were observed to significantly differ in their Lamb wave propagation. Our work attributes these variations to the same principles established in optics, in particular, refraction and reflection. Accordingly, a verification of Snell?s law was made by imaging a plate with geometry through automated laser vibrometry. A comparison was then made between the refraction angles observed in the experiment and those calculated by applying Snell?s law, where the theoretical phase velocities for each Lamb wave mode were used. Excellent agreement was found. As Lamb waves adhere to Snell?s law, ray tracing software was developed to model the effects of geometry on Lamb wave propagation. This tool is computationally quick, robust and accurate. The model can be solved in seconds allowing the user to explore designs and make changes an order of magnitude faster than finite element analysis.

15. SUBJECT TERMS **Structural Health Monitoring, Non-destructive Evaluation**					
16. SECURITY CLASSIFICATION OF:			17. LIMITATION OF ABSTRACT	18. NUMBER OF PAGES	19a. NAME OF RESPONSIBLE PERSON
a. REPORT **unclassified**	b. ABSTRACT **unclassified**	c. THIS PAGE **unclassified**	**Same as Report (SAR)**	**18**	

Standard Form 298 (Rev. 8-98)
Prescribed by ANSI Std Z39-18

Objectives: The objectives of this project are to

Aims (1): To develop a new and state-of-the-art bio-inspired concept in the design of aircraft structural components using structural health monitoring as a design criteria.

Aims (2): To persuade the aerospace industry of the efficacy of this new concept with a series of experimental test results to demonstrate the effectiveness of this new design concept on representative test articles

Aims (3): To propel structural health monitoring to the next quantum level.

Status of effort: Below describes a major component of the work performed.

1. Introduction

In-situ structural health monitoring (in-situ SHM) based on Lamb wave propagation has been a subject of many researchers' interests. The application of this technique of structural health monitoring is often restricted to either idealised structural components and/or aging infrastructures. In the latter case, the implementation of in-situ SHM is viewed as an after-thought and the concept of in-situ SHM is "forced" into the existing structural details at the fatigue critical location to provide a means of monitoring. This is certainly not optimal. To fully exploit the benefits of in-situ structural health monitoring, the application of these monitoring techniques must be addressed at the design stage. This work reported on in this report outlines a series of work that devoted to the understanding how structural geometry can be designed to facilitate the Lamb wave based structural health monitoring methodology.

This document outlines an efficient computational tool for the design of structural components with in situ structural health monitoring (In-situ SHM) in mind. In-situ SHM is an emerging area of research, primarily enabled by Lamb wave technology. Lamb waves are complex elastic guided waves which occur in plates with free boundaries. They consist of both longitudinal and transverse oscillations resulting in an elliptical displacement. Due to the complexity of these waves, they still see very little practical application. Industry favours the reliability and simplicity of well established bulk wave ultrasonics.

Authors[1,2] have previously put forward the desire to incorporate in-situ SHM into the design process rather than have it as an afterthought. Such changes would carry obvious advantages in monitoring the integrity of critical structures. One such method is to guide Lamb wave energy into critical areas for inspection. Computational modeling of the propagation of Lamb waves in plate-like structures with any geometrical details are very time consuming and costly. To aid one in designing structural details that can potentially achieve the objectives of guiding these energys into critical areas, an efficient computational tool is developed. Lamb waves can be directed by reflection and refraction just like light can. This is well established in optics. It is hoped that similar concepts can be applied to boost the probability of detection and increase the integrity of in-situ SHM without compromising a structure.

In recent years Lamb waves have demonstrated their ability to detect damage. However, the results presented by many authors require the specimen to be free of geometry [3] to avoid complications and interferences. This constrains the use of Lamb wave technology to these idealised flat structures which rarely exist in practical applications.

Plate structures with geometry were observed to significantly differ in their Lamb wave propagation. Work done attributes these variations to the same principles established in optics, in particular, refraction and reflection. Accordingly, a verification of Snell's law was made by imaging a plate with geometry through automated laser vibrometry. A comparison was then made between the refraction angles observed in the experiment and those calculated by applying Snell's law, where the theoretical phase velocities for each Lamb wave mode were used.
If Lamb waves adhere to Snell's law then ray tracing software can be developed to model the effects on geometry on Lamb wave propagation. Such tools have been widely available to model optical problems such as design of lenses. Avoiding the need to solve complicated stress fields and tensors allows for computational speed orders of magnitude greater than FEA. Furthermore the data from such a model is more intuitive to a user without the need for post processing. A user will be able to instantly observe the reasons for rays/waves altering direction when interacting with geometry. This computationally efficient tool can potentially be used to aid in the design of structural details to enhance the inspectability of the local regions using Lamb wave based inspection methodology and would also

provide means to optimise sensor placement. The achievement of these objectives will ultimately lead to the design of Lamb wave based in-situ SHM friendly structures.

The work presented comprises a set of experimental results detailing the propagation of Lamb wave in a geometrically varying flat plate. The scattering of the Lamb wave modes will be identified. A series of finite element analyses shall be presented to confirm these results. The scattering of the Lamb wave modes shall be identified. These results shall be used to demonstrate the effects of local geometry changes on the propagative characteristics of the Lamb wave modes. These results shall be analysed with the aim of determining if optic theories can be used to develop a computationally efficient technique to model and track the propagation and scattering of these dispersive wave modes. A ray tracing technique shall be presented. The potential of using this tool to guide the propagation of these Lamb wave modes to regions of interests shall be discussed therefore leading to the concept of the design for in-situ structural health monitoring.

2. Lamb wave transmission and reception

This section describes the procedures for Lamb wave transmission and reception. Transmission was achieved using piezoelectric transducers(PZT), while the Lamb waves were received using a laser vibrometer. A movable table allows positioning of the laser's scan point. This simple concept can be visualised in Figure 2.1. If the scan is repeated thousands of times across the entire specimen a complete displacement field can be captured. One such rig which allows Lamb wave imaging has been assembled in-house.

Laser vibrometry has been a key tool to aid comprehension and understanding of Lamb waves as shown by Staszewski et al[4] and Rajic et al[5]. A laser is used to detect Lamb wave displacements in a specimen rather than a PZT. This non contact approach is more precise and consistent due to the removal of coupling mediums and the pin point accuracy of the laser. The major advantage of this technique is the speed and potential for automation due to the non contact operation.

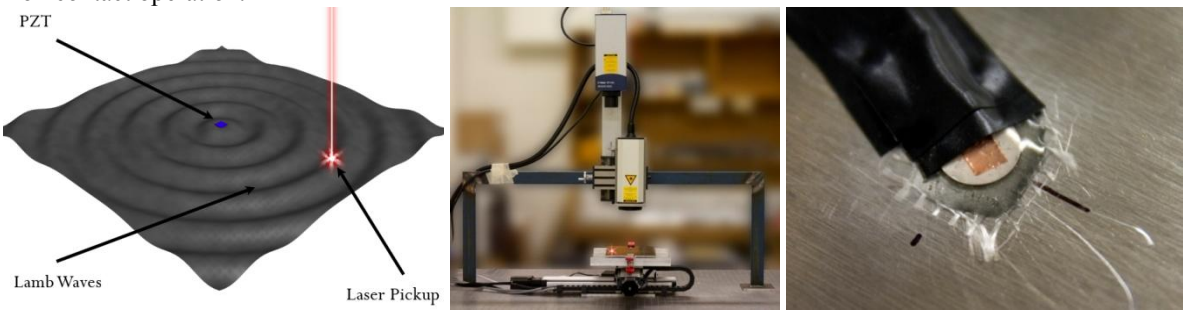

a) **b)** **c)**

Figure 2.1 a) Simplified schematic of experiment. **b)** Assembled rig. **c)** PZT transmitter.

A low profile PZT is used, 10x1mm in diameter and thickness respectively. It is produced using "Pz26" material sourced from Ferroperm. Coupling to the specimen achieved using an epoxy adhesive, while the electrical connections to the PZT are taken care by conductive copper adhesive. This is done in order to maintain a low profile and avoid heat stress involved with soldering. Figure 1 demonstrates an example.

An excitation signal was generated comprising of sine waves enclosed in a Hanning window function. Frequencies at 80 and 240 kHz were chosen for this study due to their strong resonances. This helped combat the notorious signal to noise ratios associated with laser vibrometers. Furthermore 32 ensemble averages are taken to further reduce noise. The PZT was excited through a Krohn-Hite Model 7602 broadband amplifier set to deliver peak to peak amplitude of 50V. Out of plane displacement is detected by a Polytec OFV 505 laser vibrometer. Input(displacement) and output(excitation) data is sampled at 10 and 4 MHz respectively. These rates are the maximum allowed by our National Instruments PCI-6115 data acquisition card. Motion is taken care of by a computer control X-Y table equipped with stepper motors. The ratio of the table is 5000 steps per mm providing 0.0002mm resolution.

The rig has been programmed to collect data in a zigzag pattern to reduce the duration of the experiments. The data is then rearranged to form a grid such that a complete image of the plate displacement field can be formed. Scan

points on our rig are set to 1.5mm spacing giving a point density of 1 point per 2.25mm^2. This is a great increase in density compared to the 1 point per 15.71mm^2 (420points over 110x60mm) reported by Staszewski et al[3].

3. Finite Element Setup

The specimen was modelled using the Femap pre- and post-processor, and solved in NEiNastran. Further post processing was carried out in MATLAB to convert and analyse the displacement fields from the model. From this stage onward the displacement field is identical in format to that acquired from laser vibrometry.

PZT excitation method is shown visually in the Figure 3.1 below. A disk matching the dimensions of the PZT transmitter is extruded from the plate and given the same aluminium material. A radial force is applied to this extrusion as seen below. The out of plane force can't be seen because the arrows are pointing in the negative Z direction and is hidden by geometry. Both forces are varied in time to replicate the excitation signal used in the experiment.

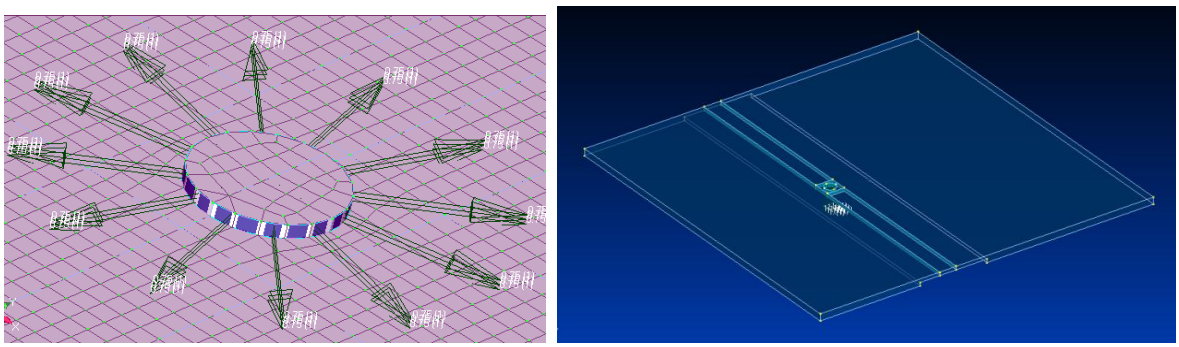

a) b)

Figure 3.1. a) excitation method **b)** refraction specimen modelled in Femap

4. Lamb Wave Reflection

One of the means of enhancing the ability to detect a defect in a known fatigue critical location is by focusing the Lamb wave energy at the desired location. When a piezoelectric element is energised in a flat plate, the Lamb wave will propagate equally in all direction. In this respect, the energy will flow to regions where it is not required. The ability to direct the energy to the desired location may enhance the ability for damage detection. To ascertain the effectiveness and the quantify the improvement achieveable by guiding the Lamb wave to a desired location, a series of finite element analyses were performed. These analyses were used to compare the detectability of a series of non-surface penetrating defect on a flat plate with and without the Lamb wave guiding feature.

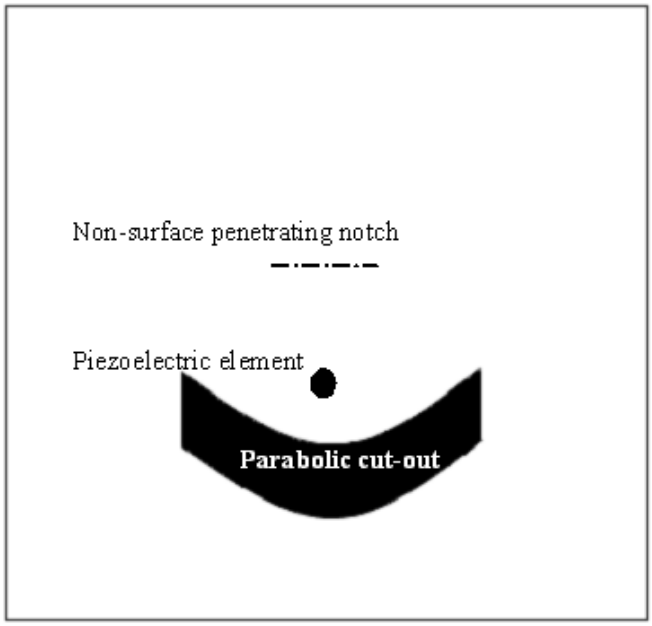

Figure 4.1: Schematic of flat plate with parabolic Lamb wave reflector

Figure 4.1 shows the schematic of the flat plate with a parabolic Lamb wave reflector. The geometry of the non-surface penetrating notch is shown in Figure 4.2. The thickness of the plate is 4 mm. In the simulations conducted, the excitation frequency of 240 kHz was used. The finite element simulations were conducted with several cut depth, d (see Figure 4.2). The results obtained were analysed in accordance to equation 4.1.

$$d_k(i,j) = \frac{\sum_{i=0}^{n_t} \left| u_k(i,j,t) - u_o(i,j,t) \right|}{n_t} \tag{4.1}$$

Where $d_k(i,j)$ is the Difference Index, $u_k(i,j,t)$ is the 2D displacement field of the k-th damage state and $u_o(i,j,t)$ is the 2D displacement field of the undamaged state.

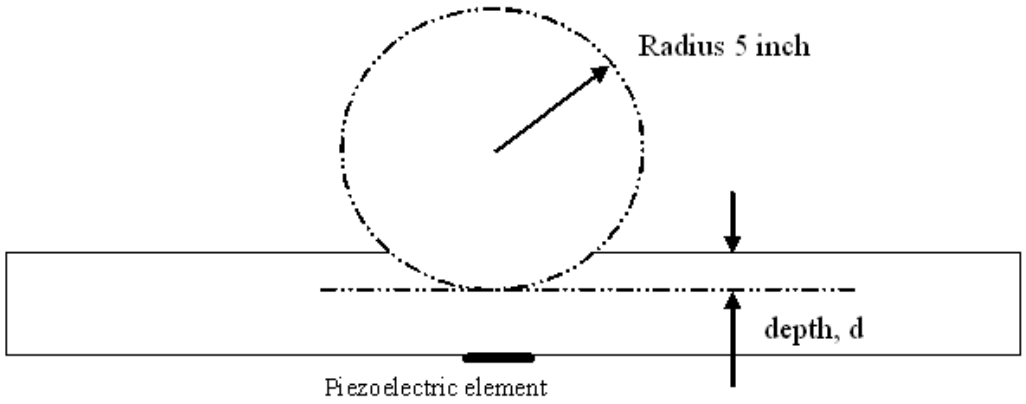

Figure 4.2 Geometry of the non-surface penetrating notch (viewed from the end of the plate)

Figures 4.3 and 4.4 show the comparison of the results obtained from a simple flat plate and that with a Lamb wave reflector. Figure 4.3(a) and 4.4(a) show the intensity of the Lamb wave over the flat plate when a fully penetrating notch was inflicted on the flat plates. It is evident from these results that intensity of the guided Lamb wave field

upstream of the notch is more uniform compared with the evenly distributed Lamb wave field on the normal flat plate.

The results presented in Figures 4.3(b) and 4.4 (b) show that the Difference Indices, $d_k(i, j)$, obtained (eqn 4.1) for the plate containing the Lamb wave reflector is significantly higher than that for the normal flat plate. The Difference Index for the concentrated Lamb wave is approximately 2 times larger. This set of results suggests that the guided Lamb wave has an enhanced detection capability.

However, the results shown in Figure 4.3 also suggest that the energy of the focussed Lamb wave is highly directional. As a result, the location of the defect with respect to the geometrical location of the Lamb wave reflector may impact on the Difference Index, and hence, its detection capability. The implications of the alignment of the defect with respect to the guided Lamb wave are shown in Figures 4.5(a) – (d). Here, the Difference Index for a given notch depth of 4.3 mm (i.e. fully penetrating notch) for the flat plate with and without the Lamb wave reflector are presented. It is evident from Figures 4.5(a) – (d) that the Difference Index is dependent on the alignment of the notch with respect to the Lamb wave concentrator. A higher Difference Index is obtained when the notch is located within the path of the guided Lamb wave. When the notch is located close to or outside of the edge of the guided Lamb wave, the Difference Index is comparable to the normal flat plate. This is expected given the intensity profile of the Lamb wave shown in Figure 4.3.

These results suggests that such geometry detail (i.e. Lamb wave reflector) when designed into a structural can enhance the detection of a defect in a given fatigue critical location. Whilst it is not practical to "cut" this into any structural component, these reflectors can be designed into structural components where a free surface exists. An example of this is the riser of a wing structure (see Figure 4.6). The free section of the riser could potentially be designed with the desired curvature instead of being traditionally straight to enhance the detection of the defect developing in the fatigue critical locations on the riser (i.e. fuel vent hole). Investigation is currently being conducted to test this hypothesis on similar structural components with free surfaces.

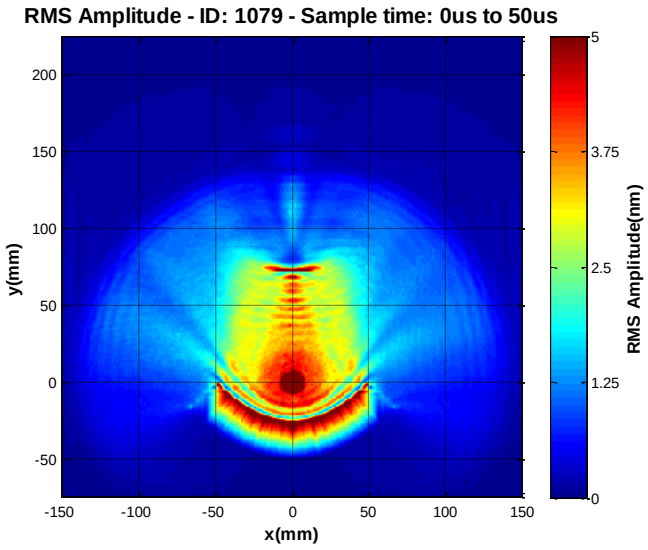

4.3(a)

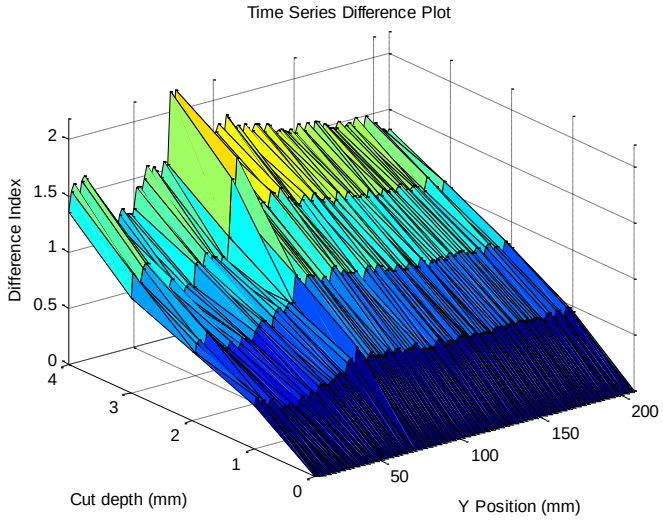

4.3(b)

Figure 4.3: Results obtained with the guided Lamb wave

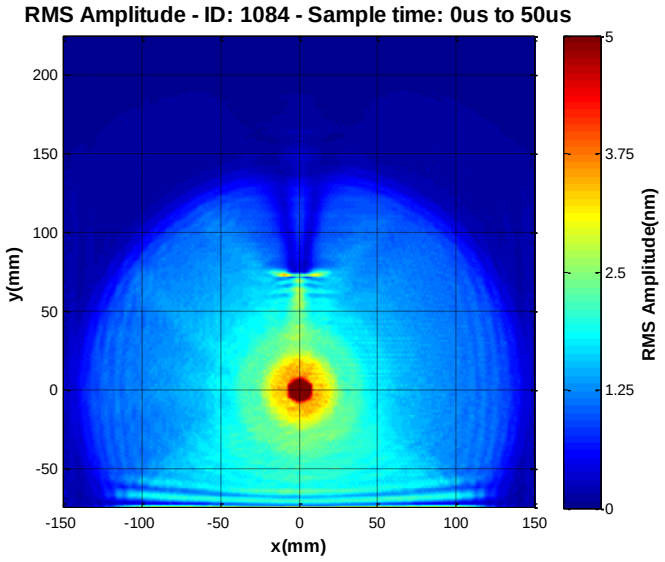

4.4(a)

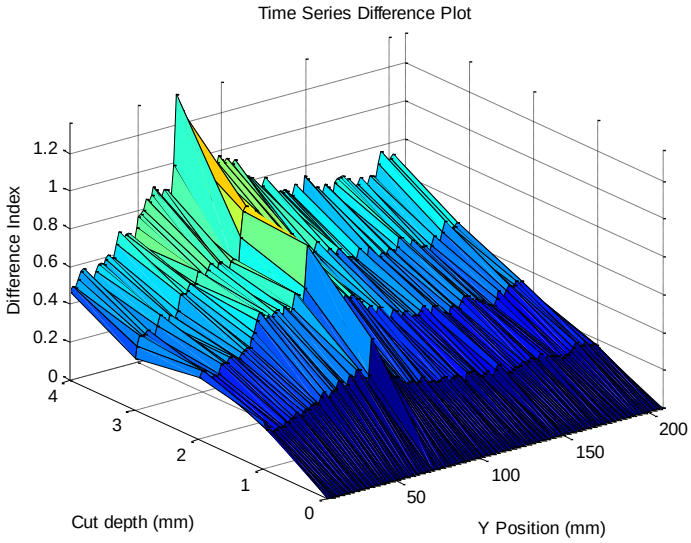

4.4(b)

Figure 4.4: Results obtained freely propagating Lamb wave

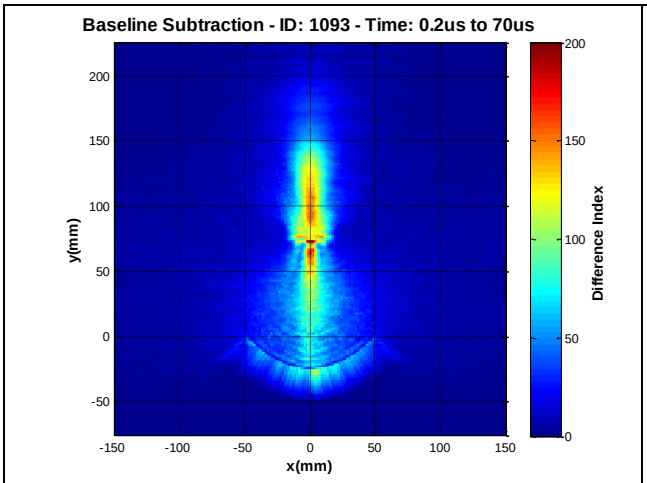

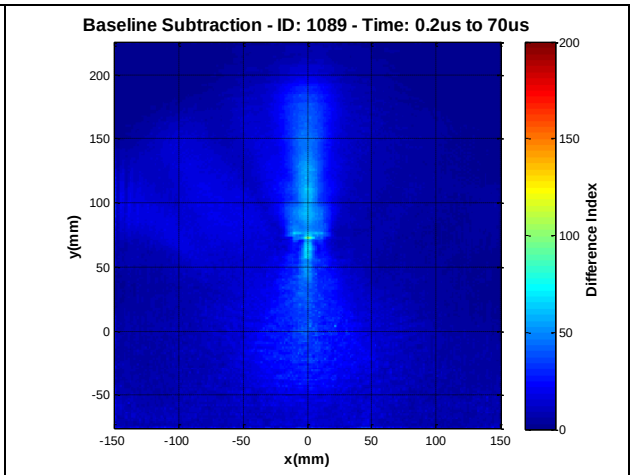

Figure 4.5(a)

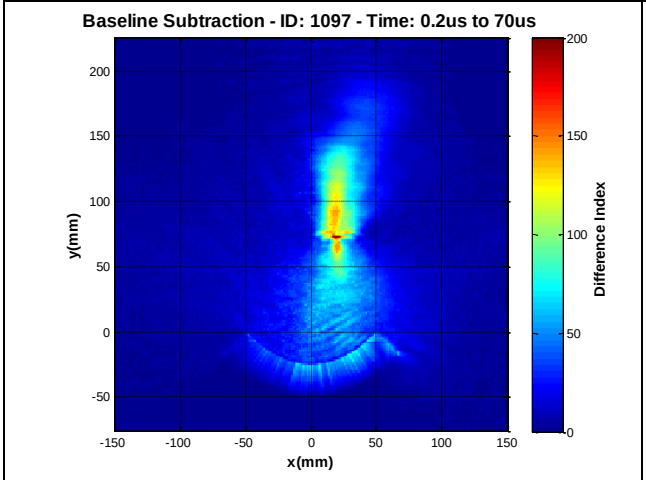

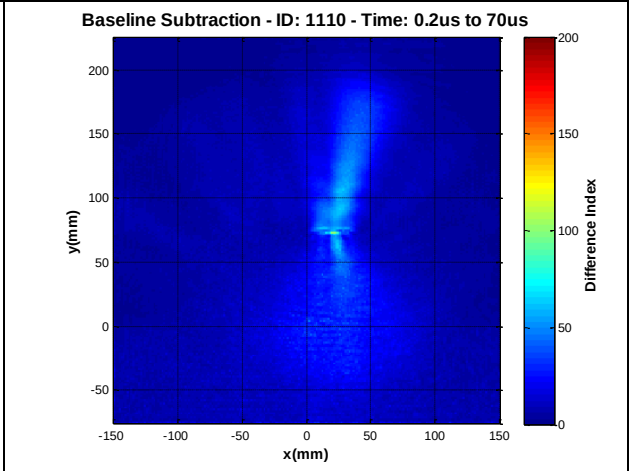

Figure 4.5(b)

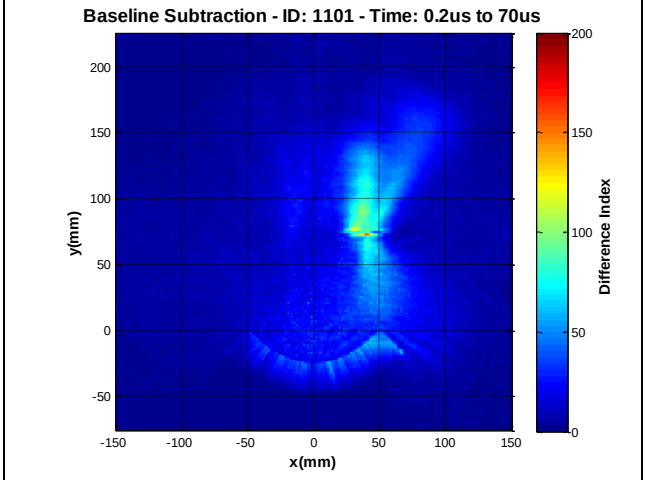

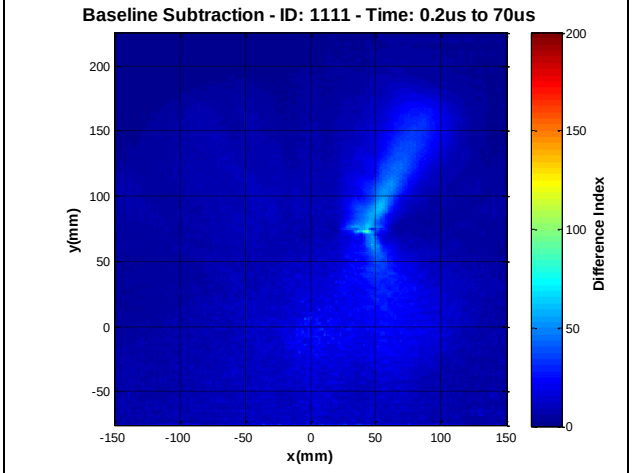

Figure 4.5(c)

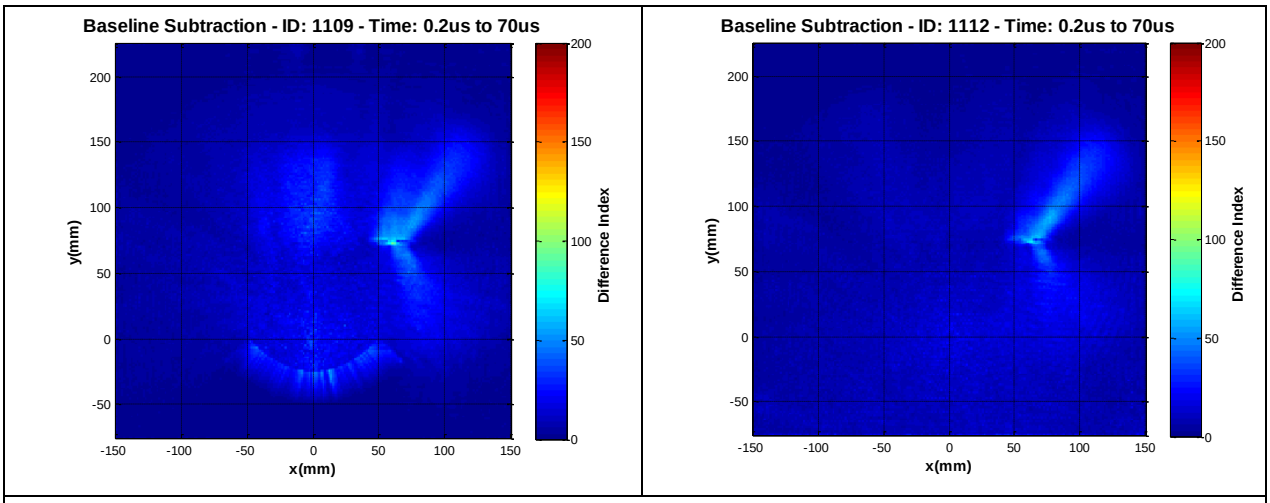

Figure 4.5(d)

Figure 4.5(a) – (d): Effects of notch location on the difference index

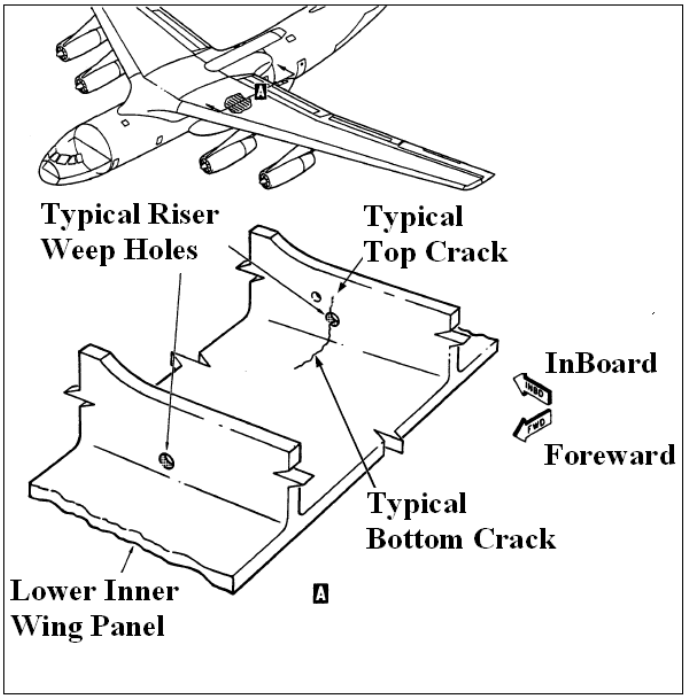

Figure 4.5: Riser section of wing panel

5. Lamb Wave Refraction

Guiding the propagating Lamb wave described in the above section may not be suitable for all fatigue critical locations. It is however expected that surface geometrical variations are expected in most fatigue critical locations (e.g. F111 underwing skin, Figure 5.1). Given that the propagating velocity of Lamb wave is dependent on plate thickness, geometry changes due to changes in thicknesses can result in the refraction of Lamb waves. This section of the report shall focus on the refraction of Lamb wave and its potential use in guiding its propagation to the fatigue critical location to enhance inspection capability.

Using finite element analyses to determine the flow of Lamb wave in a geometrically variation section of a structure is extremely expensive. To aid in the development of a design capability to visualise the propagation of Lamb wave and how they can be guided using the changing geometry, a computationally efficient optics-based tool was developed. This part of the report will demonstrate the workings of this tool and compare its efficiency against finite element analyses.

Shown in Figure 5.2a is the setup used. A 300x300x6mm aluminium plate was milled down to 3mm in the shaded blue region. The specimen was designed such that the Lamb waves would pass through a change in thickness causing them to refract. Space had to be allowed for measurement of Lamb wave propagation directions.
This specimen was analysed experimentally as well as modelled numerically. A 3 cycle Hanning windowed sine wave, with 240kHz centre frequency was used to excite Ferroperm Pz27 10x1mm round PZTs. A PZT was placed on the 6mm section as well at the 3mm to explore the Lamb wave propagation from thin-thick and thick-thin transitions.

Figure 5.1: Fatigue critical location on the F111 underwing skin

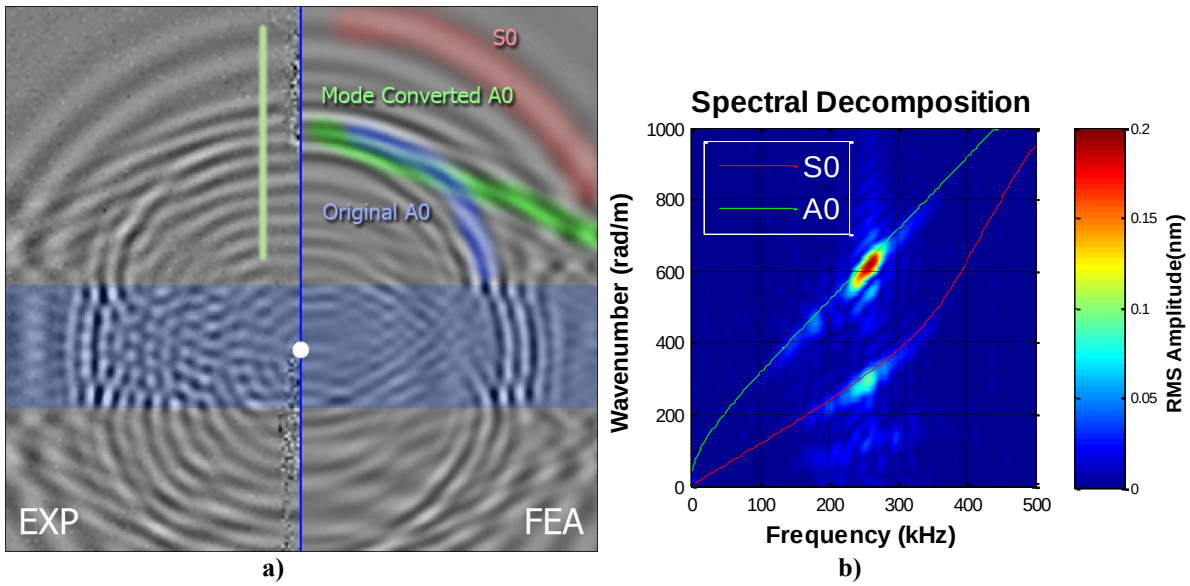

a) **b)**

Figure 5.2. a) Displacement field from specimen. **b)** 2DFFT for specimen.

Additionally Figure 5.2a demonstrates the multimodal, highly dispersive nature of Lamb waves. The use of 240kHz excitation for this system generates S0 and A0 Lamb wave modes. The spectral decomposition in Figure 5.2b highlights this and shows the amplitude for each mode. The line of data analysed by Figure 5.2b is by the light green solid line in Figure 5.1a. The 2DFFT method used in the spectral decomposition does not discriminate the mode converted A0 (MC A0) to the original A0, as they have identical wavenumbers. However inspecting the imagery in Figure 5.2a, 3 groups of waves are observable, and have been highlighted.

Image Analysis

ImageJ analysis software [6] was used to visually analyse the incident and exit angles over the thin-thick transition. The software allows angles on the image to be drawn and measurements to be taken precisely. However this is limited to the accuracy of the user's tracing. Therefore care was taken in matching the wave propagation direction perpendicular to the wavefront. Even then the result is only accurate to about +/-3 degrees due to the nature of the measurement. The θ1 measurement is more accurate perhaps to +/-0.3 degrees since we know the location of the PZT and the location of the thickness transition we simply draw a line from the PZT to any point on the transition boundary. This assumes that the wave propagates isotropically and perfectly radially. The example image in Figure 5.3 below shows S0 mode of a thick-thin FEA image been analysed. S0 is the most challenging since it is the faintest and largest wavelength mode, which results in low contrast imagery.

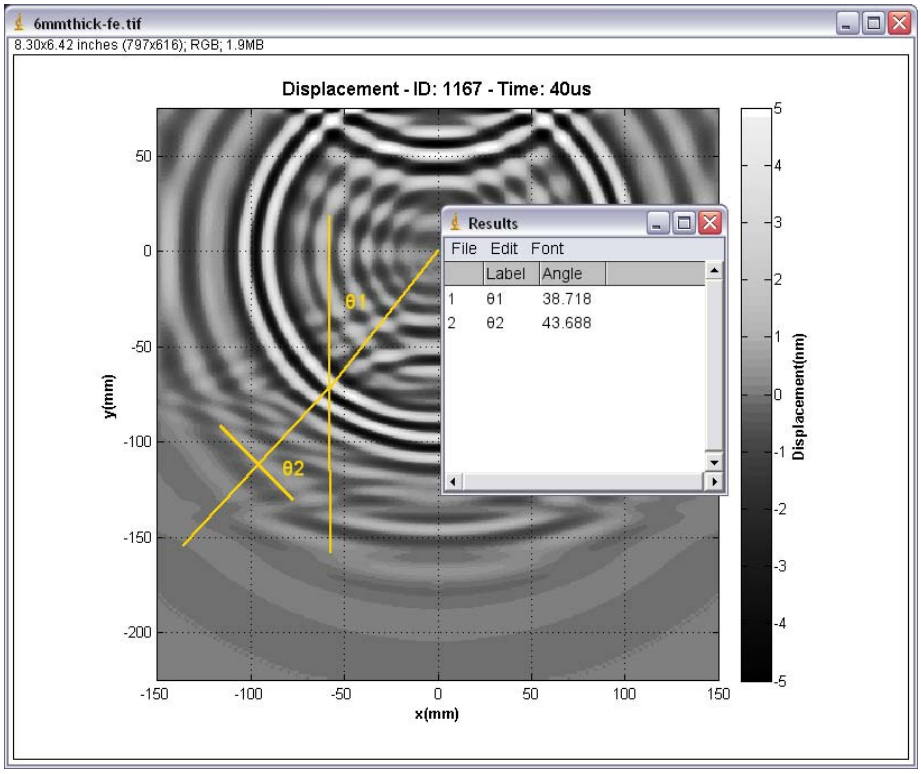

Figure 5.3. Image analysis of wavefront.

Verification of Snells Law

The theory for wave refraction states that the angles, phase velocities and index of refraction (IOR) can be related by Snells law:

$$IOR = \frac{c_1}{c_2} = \frac{\sin(\theta_1)}{\sin(\theta_2)} \qquad \text{(Equation 1)}$$

Where c and θ theta are the phase velocity and direction of propagation respectively. While subscripts 1 and 2 represent the entry and exit wave.

In order to verify this relationship the IOR for the thickness transition will be calculated through 3 different means. Results from experimental laser scans and FEA supply complete Lamb wave displacement fields. Image analysis, as explained earlier, can be performed on images generated from these displacement fields to yield entry and exit directions, θ1 and θ2 respectively. From there IOR can be simply calculated by equation 1. The third result will be calculated differently. Theoretical phase velocities are calculated by solving the fundamental Lamb wave equations presented by Viktorov [7]. These were numerically solved using commercial software called DISPERSE™.

The first set of measurements taken is presented in Figures 5.4 – 5.7 and Tables 1-4. They show the angles measured through ImageJ and the corresponding IOR. A snapshot of the displacement field is required for image analysis. In the case of where the excitation was introduced on the 3mm thick region, the snapshot was taken 32us after excitation of the PZT (Figure 5.5). This was selected as the optimum time to measure the angles as they interact with the transition in thickness. In the case where the excitation was introduced on the 6mm thick section of the test plate, the PZT was placed further from the transition requiring the snapshot to be taken later, 40us after excitation (Figure 5.7).

Following these measurements, phase velocities generated from Disperse were used in place of entry and exit angles. This provides the theoretical IOR for comparison and verification of Snell's law. Again equation 1 was used to calculate IOR. In the case of the mode converted A0 (MC A0), the entry side S0 phase velocity is used and exit side A0 phase velocity is used. Results from phase velocity changes are presented in the Tables 5-6 below. An IOR summary table (Tables 7 and 8) below shows that all cases match, including the more complicated case of the mode converted A0.

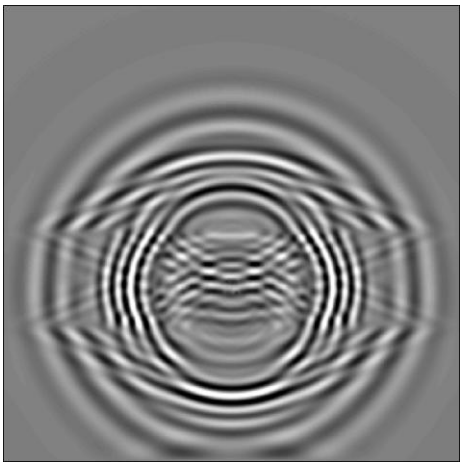

Figure 5.4. FEA thin(3mm) excitation

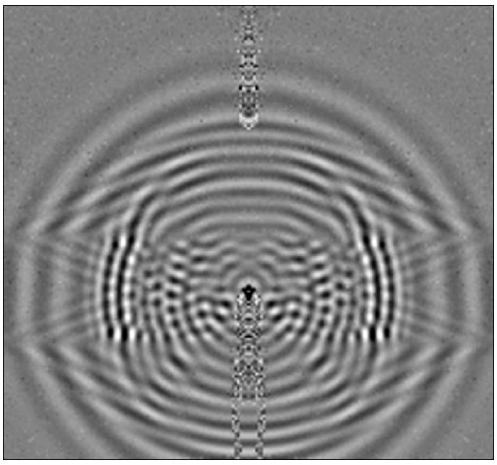

Figure 5.5. Experiment thin(3mm) excitation

Table 1. Measurements

	θ1	θ2	IOR
A0	57.995	78.906	1.16
S0	67.981	62.103	0.95
MC-A0	66.038	24.692	0.46

Table 2. Measurements

	θ1	θ2	IOR
A0	57.450	76.724	1.15
S0	63.628	59.323	0.96
MC-A0	64.144	22.782	0.43

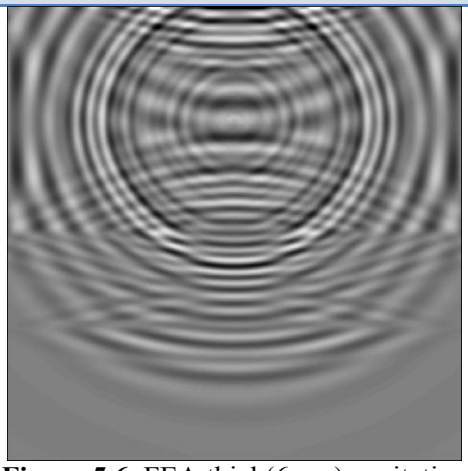

Figure 5.6. FEA thick(6mm) excitation

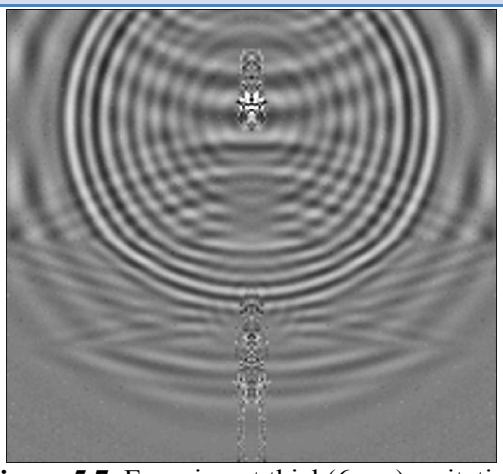

Figure 5.7. Experiment thick(6mm)excitation

Table 3. Measurements

	θ1	θ2	IOR
A0	33.254	28.217	0.86
S0	38.718	43.688	1.10
MC-A0	53.569	19.406	0.41

Table 4. Measurements

	θ1	θ2	IOR
A0	42.847	32.969	0.80
S0	37.451	43.04	1.12
MC-A0	56.575	17.769	0.37

Table 5. Disperse thin excitation

	c1(m/ms)	c2(m/ms)	IOR
A0	2.12	2.53	1.19
S0	5.39	5.21	0.97
MC-A0	5.39	2.53	0.47

Table 6. Disperse thick excitation

	c2(m/ms)	c1(m/ms)	IOR
A0	2.53	2.12	0.84
S0	5.21	5.39	1.03
MC-A0	5.21	2.12	0.41

Table 7. Thin-Thick IOR Summary

	FE	EXP	DISPERSE
A0	1.16	1.15	1.19
S0	0.95	0.96	0.97
MC-A0	0.46	0.43	0.47

Table 8. Thick-Thin IOR Summary

	FE	EXP	DISPERSE
A0	0.86	0.8	0.84
S0	1.1	1.12	1.03
MC-A0	0.41	0.37	0.41

6. Modelling Lamb Waves with Ray Tracing

Implementation

A ray trace program was written in MATLAB to model Lamb wave propagation. A key difference between ray tracer used for light rays and the one presented here is the time stepping algorithm used. Typically, in the field of modelling light, the rays are solved until a set number of reflections are attained or the rays exit the work area. This results in a fast solution which solves the completed path of a ray without consideration to the transit of the rays. In the case of Lamb wave propagation in solids the Lamb waves will never exit the workspace. Consequently the rays will always be in transit as they are bounded within the solid. Additionally the evolution and propagation of the rays are important; consequently the temporal dimension has importance. As a result the ray tracing program steps through time the same way a transient FEA simulation is done. Group velocities determine how fast the rays travel with respect to time while changes in phase velocities determine the bending of rays at thickness change interfaces.

Results

The first scenario modeled by the ray tracer is the specimen used in the verification section. Figure 6.1 shows the results obtained when the exciting piezoelectric element is located on the thin section of the plate and allow to propagate into the thicker section. The results shown in Figure 6.2 is obtained from a set of experiments where the piezoelectric element is located on the thicker section and allowed to propagate into the thinner section of the plate. In these Figures a simulated wave front based on ray tracing results were plotted over the experimental displacement field. Rays are emitted from the PZT location in a circular pattern to simulate a wave front. 360 rays per mode were emitted at 1 degree increments to form reasonable resolution in the wave front. The position of each ray is plotted as a dot resulting in a particle like representation of the wave front.

Boundaries and thickness transitions were programmed into the solver to model the plates used in earlier verifications. As described earlier there are 3 modes and therefore 3 wave fronts to simulate. Parameters for S0 and A0 modes were straightforward, they were given group and phase velocities according to their thickness. Mode converted A0 (MC A0) was emitted as a S0 wave and programmed to adopt A0 properties on any thickness transition.

The plots presented here are snapshots from a time series. Times chosen for the snapshot highlight the ability of the software to predict the wave front. Overlaying the ray trace model onto the experimental displacement field makes for an easy comparison between the two. A close match between the wave fronts predicted by the ray tracer and experiment has been found.

The results shown here do not replace currently available methods of observing Lamb wave propagation. However this method is an order of magnitude faster as shown in Table 9. This enables a user to quickly evaluate what changes occur to the wave front when alterations are made to the geometry. Similarly the location of the transducer can be altered quickly to reveal the effects of sensor location.

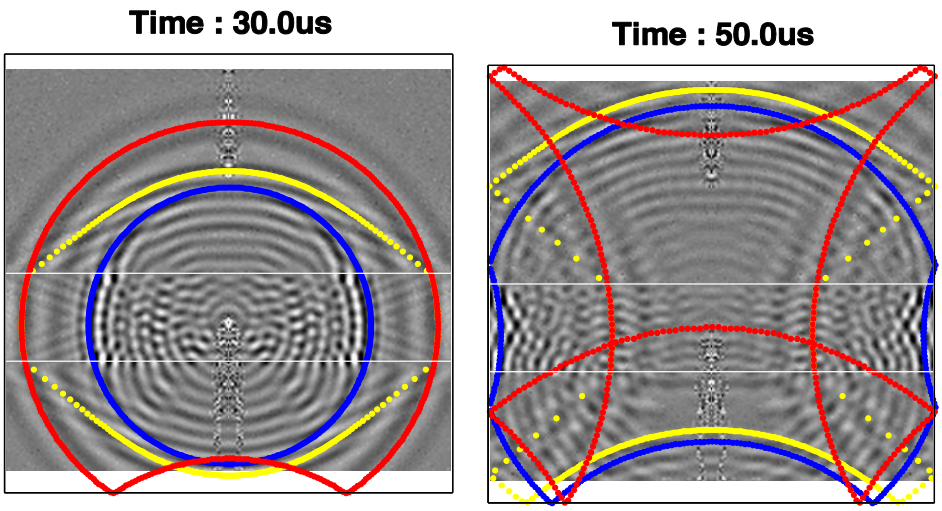

Figure 6.1. Simulated wave front overlaid on experimental displacement field. red – S0, blue – A0, yellow – mode converted A0 (MC A0).

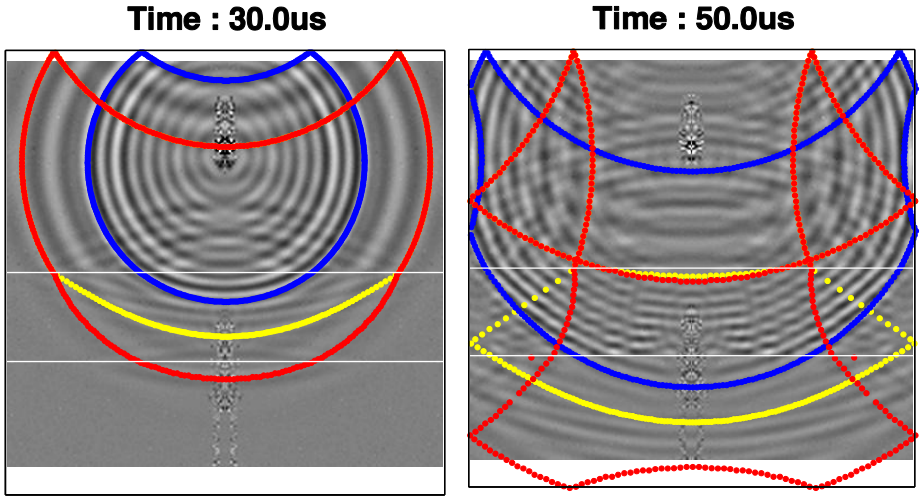

Figure 6.2. Simulated wave front overlaid on experimental displacement field. red – S0, blue – A0, yellow – mode converted A0.

Table 9. Performance comparison

Method	Solution Time
Ray trace solver	154 seconds per mode
Laser Vibrometry	8 hours + Fabrication
FEA - NeiNastran	7 hours 45 minutes

Mode Preference For Wave Redirection

Original A0 (not mode converted) appears to be the most desirable mode to guide because:

- S0 mode has an IOR of 0.97 making it difficult to alter direction. Additionally energy is lost through mode conversion at thickness transitions.
- Mode converted A0 (MC A0) has very high IOR lending itself to easy direction changes. From thin to thick it has a sizable signal/amplitude. However from thick to thin mode converted A0 is very weak and unusable.
- Original A0 has a low IOR but is usable and holds well through the thickness transitions.

However if we are guiding waves on a flat plate we are most likely going to use a raised ribbing structures to guide the wave. In this case the Lamb waves will undergo a thin-thick-thin transition. Mode converted A0 is quite strong

on the thin to thick transition therefore it may be possible to target mode converted A0. This would result in milder geometry and a more compact lens.

Wave Redirection

The ray tracing software was used to design a lens which targets a single mode and directs it to converge at a focal point. It is envisaged that the redirection of waves will help to enhance displacement amplitude and detectability of defects. This exercise demonstrates the initial goal of this research, to provide a fast design tool which gives the user instant feedback with respect to design changes.

Again the excitation frequency is set to 240kHz, while 3mm and 6mm thicknesses are used, thereby retaining the same Lamb wave modes used earlier. In order to better visualise the redirection of waves, the ray tracing software was altered to plot the rays of propagation from the time of emission.

The lens combination shown in Figure 6.3 consists of a crescent shaped lens and a concave lens. This combination is used to target the mode converted A0 (MC A0) originating from incident S0. The crescent's initial convex shaped transition causes the mode converted A0 (MC A0) to converge. Once the mode conversion occurs the wave behaves as an A0 and therefore concave shaped transitions are used to further converge the wave. The ray tracing tool was used to iteratively refine the positioning and curvature of each element.

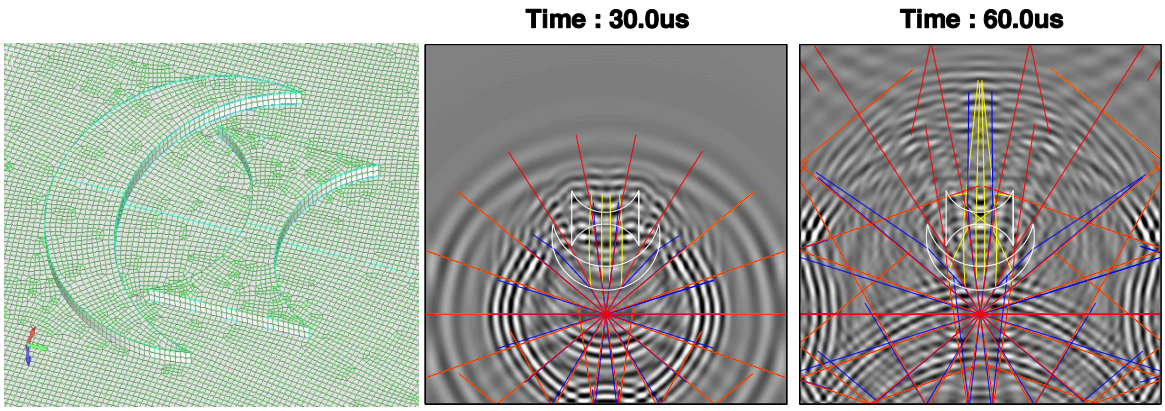

Figure 6.3. Lamb wave lens with 2 elements targeting mode converted A0.

Figure 6.3 shows the ray trace model overlaid onto the displacement field solved by an FEA model of the lens geometry. It is evident that geometrical details can be designed toto effectively redirect and converge the waves. Comparing the incident A0 to the focused mode converted A0 (MC A0) in figure 11, it is also evident that these technique can also give rise to the losses and reflections caused by each thickness transition. The application of this computationally efficient tool can be used investigate how geometrical details in local regions can affect the propagation of the Lamb wave energy. It can also be used to guide in the placement of piezoelectric elements to generate and receive the lamb wave modes for inspection. As part of the proof of concept of the design for in-situ structural health monitoring, this tool is currently being used to investigate the implications of re-designing of local geometric features in a fatigue critical location on the underwing skin of the F111.

7. Discussions

The results presented above shows that structural features can be build designed into a structural component to guide the propagation of Lamb wave for structural health monitoring. This is especially important when the issue of hot-spot monitoring is desired. The design of structural features can be aided with the efficient ray-tracing technique presented above. The computationally more expensive modelling attempts can be made with the proposed structural details.

The work presented above suggests that, depending on the structural features, the reflection and refraction of Lamb waves can potentially be used to enhance the design of structural component making them more amenable to in-situ structural health monitoring using the wave propagation methodology.

Work is currently being performed to "re-design" the local geometry to enhance the detection of the following structural sections;

1. Riser section of an aircraft structure with a fatigue critical location at the fuel vent hole
2. Fatigue critical location at the F111 underwing skin

8. Conclusion

The work presented above has demonstrated that;

(i) the guided Lamb wave can potentially be used to direct the energy of Lamb wave to the desired location of the structure

(ii) the wave fronts will bend according to the phase velocities of the wave mode as described by Snell's law.

(iii) An efficient analysis tool has been developed to aid with the optimization of flow of Lamb wave energy into a desired location within a structure

Finite element simulations and laser vibrometry experiments have been used to substantiate the findings in this report. Following verification a custom program was written to simulate Lamb wave propagation. The same plate specimens were simulated using this program. Subjective comparisons were made between experimental results and ray traced wave fronts. Excellent agreement and accuracy was found showing that ray tracing can successfully predict the shape of wave fronts.

Returning to the goal of designing for structural health monitoring by guiding and redirecting waves the ray tracing tool was applied to design lens geometry to focus Lamb waves. The lens shape and positions were optimised using the tool while FEA followed to confirm its effectiveness and agreement.

The tools described in the above can be used as a visualization and a comprehension tool. It may also be used as a fast design tool to determine the effect of geometry on the propagation of Lamb waves. Used carefully this could aid sensor placement and evaluate alterations to geometry. However the technique is in its infancy and there are many extensions possible. It can be modified to predict the time of flight in variable thickness structures which may lend itself to defect triangulation [8]. Future work may involve programming of attenuation rays according to time, distance and thickness transitions. Such development may allow for prediction of Lamb wave energy distribution in complex plate structures. This would allow quick evaluation of a structure's in-situ SHM friendliness as well as a greater aid in sensor placement.

References:

1. F. K. Chang, Intelligent sensor networks can cut maintenance cost, downtime, ReliablePlant **5012** (3) (2007).
2. C. K. W. Wong, W. K. Chiu, N. Rajic and S. C. Galea, Can stress waves be used for monitoring of sub-surface defects in repaired structures? Composite Structures **76** (3), 199-208 (2006).
3. Staszewski, W.J., et al., *Structural health monitoring using scanning laser vibrometry: I. Lamb wave sensing.* Smart Materials & Structures, 2004. **13**(2): p. 251-260.
4. W. J. Staszewski, B. C. Lee, L. Mallet and F. Scarpa, Smart Materials & Structures **13** (2), 251-260 (2004).
5. *N. Rajic, S.. Galea, C.Rosalie.*, *A Feasibility Study into the Active Smart Patch Concept for Composite Bonded Repairs*. 2008, Defence Science and Technology Organisation.
6. Staszewski, W.J., B.C. Lee, and R. Traynor, *Fatigue crack detection in metallic structures with Lamb waves and 3D laser vibrometry.* Measurement Science & Technology, 2007. **18**(3): p. 727-739.
7. Viktorov, I.A., *Rayleigh and Lamb waves: physical theory and applications*. Ultrasonic technology. 1967, New York,: Plenum Press. x, 154 p.
8. Lu, Y., L. Ye, and Z.Q. Su, *Crack identification in aluminium plates using Lamb wave signals of a PZT sensor network.* Smart Materials & Structures, 2006. **15**(3): p. 839-849.

Abstract: A significant amount of research work has been dedicated towards structural health monitoring. Most of these works are targeted towards the introduction of these monitoring techniques to existing structures. To fully exploit the benefits of structural health monitoring, the application of these monitoring techniques must be addressed at the design stage. The work reported on in this report outlines a series of work that devoted to the understanding how structural geometry can be designed to facilitate the Lamb wave based structural health monitoring methodology. This report also describes a computationally efficient optical approach to studying the propagation of Lamb waves in a plate-like structure. This analytical tool shall be used to visualise the flow of the Lamb wave

energy to aid in the design of geometrically varying structural features for efficient structural health monitoring. Compared with flat plates, plate-like structures with geometry were observed to significantly differ in their Lamb wave propagation. Our work attributes these variations to the same principles established in optics, in particular, refraction and reflection. Accordingly, a verification of Snell's law was made by imaging a plate with geometry through automated laser vibrometry. A comparison was then made between the refraction angles observed in the experiment and those calculated by applying Snell's law, where the theoretical phase velocities for each Lamb wave mode were used. Excellent agreement was found. As Lamb waves adhere to Snell's law, ray tracing software was developed to model the effects of geometry on Lamb wave propagation. This tool is computationally quick, robust and accurate. The model can be solved in seconds allowing the user to explore designs and make changes an order of magnitude faster than finite element analysis (FEA).

Personnel Supported: A PhD student (Wern Han ONG) is supported with this proposal

Publications: We are currently preparing 1 paper for Structural Health Monitoring – an International Journal; and 1 paper for the Asia-Pacific Workshop on Structural Health Monitoring (Tokyo, Nov 2010).

Interactions: Participation in International Workshop on Structural Health Monitoring (Sep 2009).

Inventions:

None

Honors/Awards: None

Archival Documentation: The papers, when submitted will be copied onto Dr Kumar Jata.

Software and/or Hardware (if they are specified in the contract as part of final deliverables): None